LANGMUIR

pubs.acs.org/Langmuir Article

Lipid Hydroperoxide Compromises the Membrane Structure Organization and Softens Bending Rigidity

Gustavo Scanavachi, Ana Coutinho, Alexander Andreevich Fedorov, Manuel Prieto, Ana M. Melo,* and Rosangela Itri*

Cite This: *Langmuir* 2021, 37, 9952−9963 Read Online

ACCESS | Metrics & More | Article Recommendations | Supporting Information

ABSTRACT: Lipid hydroperoxides are key mediators of diseases and cell death. In this work, the structural and dynamic perturbations induced by the hydroperoxidized POPC lipid (POPC-OOH) in fluid POPC membranes, at both 23 and 37 °C, were addressed using advanced small-angle X-ray scattering (SAXS) and fluorescence methodologies. Notably, SAXS reveals that the hydroperoxide group decreases the lipid bilayer bending rigidity. This alteration disfavors the bilayer stacking and increases the swelling in-between stacked bilayers. We further investigated the changes in the apolar/polar interface of hydroperoxide-containing membranes through time-resolved fluorescence/anisotropy experiments of the probe TMA-DPH and time-dependent fluorescence shifts of Laurdan. A shorter mean fluorescence lifetime for TMA-DPH was obtained in enriched POPC-OOH membranes, revealing a higher degree of hydration near the membrane interface. Moreover, a higher microviscosity near TMA-DPH and lower order are predicted for these oxidized membranes, at variance with the usual trend of variation of these two parameters. Finally, the complex relaxation process of Laurdan in pure POPC-OOH membranes also indicates a higher membrane hydration and viscosity in the close vicinity of the −OOH moiety. Altogether, our combined approach reveals that the hydroperoxide group promotes alterations in the membrane structure organization, namely, at the level of membrane order, viscosity, and bending rigidity.

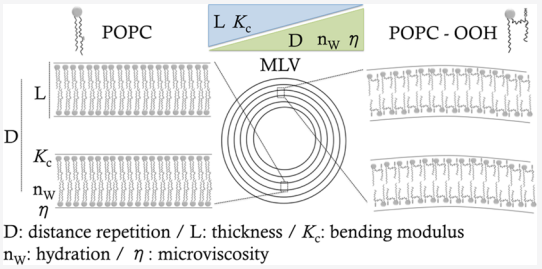

D: distance repetition / L: thickness / K_c: bending modulus
n_W: hydration / η : microviscosity

INTRODUCTION

Lipid membranes are composed of a variety of lipids including unsaturated and polyunsaturated fatty acids (PUFAs), sphingolipids, and sterols, whose distribution in the inner and outer leaflets defines important biophysical membrane features as spontaneous curvature, bending rigidity, fluidity, and permeability, among others. Furthermore, temperature-dependent packing of different lipid species in the membrane may favor lipid demixing into domains, which harbor key proteins associated with signaling mechanisms and cell homeostasis. In spite of their importance, unsaturated lipids, PUFAs, and sterols are vulnerable to peroxidation either by enzymatic or non-enzymatic mechanisms.[1−3] As a consequence, chemical structure modifications imposed by lipid peroxidation can alter membrane biophysical properties,[4,5] leading to cell homeostasis loss and eventually to cell death depending on the oxidative damage level.[6]

Notably, lipid hydroperoxides have been recently recognized as key mediators of diseases and cell death.[7,8] To date, many theoretical and experimental studies provided information on membrane properties and structural organization of lipid hydroperoxide-containing bilayers. Since the hydroperoxide has a more hydrophilic character in respect to the lipid acyl chain, the oxidized tail bends toward the bilayer surface, exposing the OOH group to the polar milieu,[9,10] promoting an increase in the lipid molecular area. Herein, we investigate lipid bilayer properties containing an increasing amount of 1-palmitoyl 2-oleoyl-phosphatidylcholine hydroperoxide (POPC-OOH) (Figure 1). In particular, previous micropipette experiments on POPC-OOH giant unilamellar vesicles (GUVs) determined an increase of 15% in the area excess in respect to non-oxidized 1-palmitoyl-2-oleoyl-*sn*-glycero-3-phosphocholine (POPC) membranes.[11] This effect was later confirmed by small-angle X-ray scattering (SAXS) data analysis[12] and found to be accompanied by membrane thickness reduction.[12,13] Interestingly, accumulation of POPC-OOH in the membrane does not change its permeability,[11] although the hydroperoxidized lipid bilayer becomes more susceptible to electroporation.[14−16] Further, liquid disordered (Ld)/liquid ordered (Lo) phase separation has also been observed in a 1,2-dipalmitoyl-*sn*-glycero-3-phosphocholine (DPPC)/POPC-OOH/cholesterol system, showing that POPC-OOH can modulate lipid domains.[5]

Received: March 24, 2021
Revised: July 22, 2021
Published: August 10, 2021

https://doi.org/10.1021/acs.langmuir.1c00830
Langmuir 2021, 37, 9952−9963

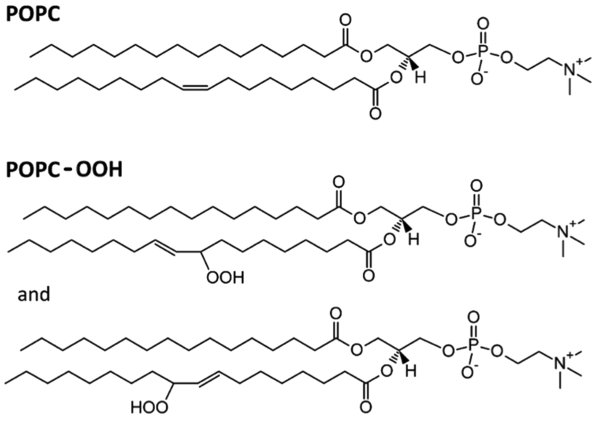

Figure 1. Chemical structures of 1-palmitoyl-2-oleoyl-*sn*-glycero-3-phosphocholine (POPC) and the two isomers of 1-palmitoyl-2-oleoyl-phosphatidylcholine hydroperoxide (POPC-OOH).[11] The mixture of the isomers is referred to as POPC-OOH throughout the paper.

Concerning the excess of membrane area promoted by the hydroperoxide lipid, micropipette assays on POPC-OOH GUVs also revealed a significant decrease in the stretching modulus that reduced from 200 mN m^{-1} for POPC membranes to 50 mN m^{-1} for POPC-OOH lipid bilayers without compromising membrane integrity.[11] Enhanced membrane undulations have also been detected upon the influence of POPC-OOH,[17] but no bending modulus evaluation has been made so far.

In this regard, the current work aims to gather new information about the membrane surface properties of POPC vesicles with increasing amounts of POPC-OOH. Membrane bending rigidity, surface hydration properties, and order parameters are intensively examined by SAXS and advanced time-resolved fluorescence techniques to better understand the impact of the hydroperoxidized lipid on the membrane structure at the molecular level.

EXPERIMENTAL SECTION

Materials. POPC was purchased from Avanti Polar Lipids (Alabaster, AL) and hydroperoxidized POPC (herein termed as POPC-OOH) was produced as described elsewhere.[11] Figure 1 shows the chemical structures of POPC and POPC-OOH. The fluorescent probes, 1-(4-trimethylammoniumphenyl)-6-phenyl-1,3,5-hexatriene *p*-toluenesulfonate (TMA-DPH) and 6-dodecanoyl-2-dimethylamino-naphthalene (Laurdan), were obtained from Invitrogen Thermo Fisher (Leiden, The Netherlands). All organic solvents were of UVASOL grade from Merck (Darmstadt, Germany). Other chemicals were of analytical or spectroscopic grade and were used without further purification. Buffers were prepared using Milli-Q water (Millipore, USA).

Preparation of Lipid Vesicles. Multilamellar vesicles (MLVs) and large extruded vesicles of POPC with increasing molar ratios of POPC-OOH (POPC-OOHχ, 0−100%) were prepared as previously described.[18,19] Briefly, chloroform stock solutions of both lipids were combined in appropriate amounts to yield a final concentration of 0.1, 0.5, or 10 mM for TMA-DPH, Laurdan, and SAXS experiments, respectively. The fluorescent probes (also in chloroform) were cosolubilized prior to solvent evaporation at a probe:lipid ratios of 1:200 (for TMA-DPH) and 1:100 (for Laurdan). The organic solvent was then first evaporated under a stream of nitrogen and further under vacuum for at least 4 h. The dry lipid films were hydrated in 10 mM HEPES, 150 mM NaCl (pH 7.0), and 0.2 mM EDTA buffer for 30 min and then re-equilibrated by 10 freeze−thaw cycles to obtain MLVs. The resulting lipid suspensions were further extruded through 100 nm pore diameter polycarbonate membranes in an Avanti Mini-Extruder system, repeated 31 times. It is usually assumed that such a procedure produces large unilamellar vesicles (LUVs). However, as it will be concluded from the SAXS results presented ahead in the text, extruded POPC/POPC-OOHχ vesicles with χ = 0, 10, 25, 30, 50, and 70 mol % display diffraction peaks characteristic of few bilayer stacking. For this reason, here, we refer to these vesicles as extruded vesicles.

The exact concentrations of POPC and POPC-OOH stock solutions were confirmed by the phosphorus analysis.[20] The concentrations of the chloroform stock solutions of the fluorescent probes were determined spectrophotometrically using molar extinction coefficients of 52 × 10^3 M^{-1} cm^{-1} at 355 nm for TMA-DPH[21] and 19.5 × 10^3 M^{-1} cm^{-1} at 360 nm for Laurdan.[22]

SAXS. SAXS experiments were performed at the Brazilian Synchrotron Light Laboratory (LNLS, Campinas, Brazil). The scattering vector modulus $q = 4\pi\sin\theta_{SAXS}/\lambda$, with $2\theta_{SAXS}$ being the scattering angle and λ being the X-ray wavelength of 1.548 Å, ranged from 0.013 to 0.50 $Å^{-1}$. Samples were placed in a 1 mm path length mica holder and the exposition time was 300 s.

The scattering intensity, $I(q)$, from a large vesicle, where the lipid bilayer thickness is much smaller than its size, can be described as a product of a structure factor, $S(q)$, and a form factor, $P(q)$, such as:[23,24]

$$I(q) = P(q)S(q) = \frac{2\pi A}{q^2}P_t(q)S(q) \tag{1}$$

with A being the area of the basal plane, and $P_t(q)$ the form factor of the lipid bilayer cross section perpendicular to the A plane.

Extruded Lipid Vesicles. $P_t(q)$ contains information about the lipid bilayer structure and it is here modeled as step functions with three different electron densities (ρ) in respect to the electron density of the buffer (ρ_{buf} = 0.34(2) e/Å^3).[25,26] These regions are characterized by their electron densities ρ and thicknesses R from the center of the bilayer toward the aqueous solution as (i) a methyl region (ρ_{CH3}, R_{CH3}), (ii) a CH_2 chains-containing inner lipid bilayer medium (ρ_{CH2}, R_{CH2}), and (iii) an outer membrane containing polar headgroups and solvation molecules (ρ_{pol}, R_{pol}):[27]

$$P_t(q) = \left[\frac{2}{q}\{\Delta\rho_{CH3}\sin(qR_{CH3}) + \Delta\rho_{CH2}\{\sin[q(R_{CH2}+R_{CH3})] - \sin(qR_{CH3})\} + \Delta\rho_{pol}\{\sin[q(R_{pol}+R_{CH2}+R_{CH3})] - \sin[q(R_{pol}+R_{CH2})]\}\}\right]^2 \tag{2}$$

with

$$\Delta\rho_{CH3} = \rho_{CH3} - \rho_{buf},\ \Delta\rho_{CH2} = \rho_{CH2} - \rho_{buf},\ \text{and}\ \Delta\rho_{pol} = \rho_{pol} - \rho_{buf} \tag{3}$$

$S(q)$ in eq 1 is equal to 1 for non-interacting systems as in the case of LUVs. For MLVs, $S(q)$ takes into account the correlation between stacked bilayers.

During the analysis, we noticed that the SAXS data are due to two distinct contributions, namely, (i) scattering from LUVs and (ii) scattering from a few stacked bilayers depending on the POPC-OOH amount in the membrane. In this way, we use the following equation to analyze the experimental data from extruded vesicles:

$$I(q) = \gamma P(q) + (1-\gamma)(P(q)\cdot S(q)) \tag{4}$$

with γ being the fraction of LUVs with the form factor $P(q)$ and $(1-\gamma)$ being the fraction of stacked lipid bilayers where each bilayer has the same scattering density profile, and hence, $P(q)$, as that of LUVs; $S(q)$ was calculated considering the modified Caillé theory (MCT)[28] such as:[27]

https://doi.org/10.1021/acs.langmuir.1c00830
Langmuir 2021, 37, 9952−9963

$$S(q) = N + 2\sum_{n_o-1}^{N-1}(N - n_o)\cos(qn_oD_{rep})e^{-0.0435q^2D_{rep}^2\eta_{Caillé}} \quad (5)$$

where N is the number of stacked bilayers, n_o is the order, D_{rep} is the repetition distance between two bilayers, which includes the bilayer thickness plus hydration layer, and finally, $\eta_{Caillé}$ is the Caillé parameter related to the bending fluctuations of the membrane.

A global fitting procedure was employed to fit concomitantly the whole set of SAXS data (eq 4) from POPC/POPC-OOHχ extruded vesicles (with χ varying from 0 to 100 mol %) using the GENFIT software.[29]

The $P_t(q)$ fitting parameters are constrained as a linear combination of those associated with single vesicle compositions of POPC and POPC-OOH as

$$R_i = \chi R_i(\text{POPC} - \text{OOH}) + (1 - \chi)R_i(\text{POPC}) \quad (6)$$

$$\rho_i = \chi\rho_i(\text{POPC} - \text{OOH}) + (1 - \chi)\rho_i(\text{POPC}) \quad (7)$$

with i corresponding to CH3, CH2, and polar head regions (eqs 2 and 3).

The electron density profiles were then determined for each extruded vesicles prepared with varying POPC-OOH amounts, where the transitions between the step levels were smoothed by error functions.[30]

Non-extruded Lipid Vesicles. The study of MLVs allowed us to quantify the bending modulus, K_c, for POPC and the whole set of hydroperoxidized membranes from the analysis of diffraction peaks via MCT (eq 5), where the Caillé parameter is defined as:[28]

$$\eta_{Caillé} = \frac{\pi k_B T}{2D_{rep}^2\sqrt{K_c B}} \quad (8)$$

with k_B being the Boltzmann constant, T being the temperature, and B being the compression modulus between two adjacent bilayers.[28] Of note, we noticed that the MLV diffraction peaks are split in three major components with slight differences in D_{rep} values due to the salt effect from the buffer.[31] Accordingly, the scattering intensity $I(q)$ modeling to the MLV experimental data were done, taking into account MCT as:

$$I(q) = P(q)[a_1S_1(q) + a_2S_2(q) + a_3S_3(q)] \quad (9)$$

with $a_1 + a_2 + a_3 = 1$. Figure S1 shows an example of the $S(q)$ decomposition modeling to a POPC SAXS curve. In this approach, we assume that the bilayer structure is not affected by the salt distribution,[31] and hence, $P(q)$ form factors from non-extruded vesicles with χ varying from 0 to 100 mol % POPC-OOH have the same scattering density profiles as those retrieved from the fittings to the SAXS data from experimental extruded vesicles. Furthermore, according to eqs 5 and 9, three D_{rep} values were obtained from the fitted $S(q)$ functions (eq 9) and the number of bilayers, N, and the $\eta_{Caillé}$ values were the same for each lipid composition. Averaged values were considered to calculate the bending modulus K_c. Similar to the extruded lipid vesicles, a global fitting procedure within the GENFIT software[29] was used to analyze concomitantly all data from MLVs.

Steady-State Fluorescence Spectroscopy. Steady-state fluorescence experiments were carried out with an SLM-AMINCO 8100 spectrofluorometer (SLM Instruments Inc., Urbana, IL) in a right-angle geometry, equipped with double excitation/emission monochromators and automated rotating Glan-Thompson polarizers. The light source was a 450 W Xe arc lamp and the reference was a rhodamine B quantum counter solution. All measurements were performed in 5 × 5 mm quartz cuvettes (Hellma Analytics) under constant magnetic stirring and a controlled temperature of 23 or 37 °C (± 0.2 °C) using a Julabo F25 circulating water bath.

The emission spectra of TMA-DPH and Laurdan were recorded with excitation at 340 and 350 nm, respectively. For TMA-DPH fluorescence anisotropy measurements, samples were excited at 340 nm and the polarized emission was detected at 430 nm. The steady-state fluorescence anisotropy, $\langle r\rangle$, was calculated as:[32]

$$\langle r\rangle = \frac{I_{VV} - G\cdot I_{VH}}{I_{VV} + 2\cdot G\cdot I_{VH}} \quad (10)$$

where the intensities I_{VV} and I_{VH} are the vertical and horizontal components of the polarized fluorescence emission, when the sample is excited with vertically polarized light, respectively. The G factor ($G = I_{HV}/I_{HH}$, components with horizontal excitation) accounts for the transmission efficiency of the monochromator to the polarization of light. Blank subtraction was always taken into account. Data are presented as mean ± standard deviation of at least three independent experiments (with 10 measurements for each sample).

Time-Resolved Fluorescence Spectroscopy. Time-resolved fluorescence intensity and anisotropy measurements were performed by the time-correlated single-photon timing technique at both 23 and 37 °C as previously described.[18,33] Briefly, both TMA-DPH and Laurdan probes were excited at 340 nm using a frequency doubled secondary cavity-dumped dye laser of DCM (Coherent 701-2). The fluorescence emission was recorded at 430 nm for TMA-DPH, and a series of emission wavelengths from 400 up to 540 nm with a 10 nm step was used for Laurdan. The fluorescence was detected using a Jobin-Yvon HR320 monochromator with a cutoff filter to avoid interference from Rayleigh-scattered light and using a Hamamatsu R-2809U microchannel plate photomultiplier. The fluorescence intensity decays, $I(t)$, were acquired with the emission polarizer set at 54.7° (the magic angle) relative to the vertically polarized excitation beam. For TMA-DPH anisotropy decays, the parallel and perpendicular polarized components of the fluorescence ($I_{VV}(t)$ and $I_{VH}(t)$, respectively) to the plane of excitation light were alternatively collected. The instrument response function (IRF) was obtained from the excitation light scattered by a Ludox solution (silica, colloidal water solution, Aldrich). The IRF and fluorescence intensity decays were acquired in a multichannel analyzer with a time window of 1024 channels up to 50,000 and 20,000 counts in the peak channel, respectively.

Fluorescence Decay Analysis. Fluorescence decay analysis was performed using the TRFA Data Processing Package (version 1.4) from the Scientific Software Technologies Center (Belarusian State University). The goodness of fit was evaluated by the reduced χ^2 value (<1.3) and a random distribution of weighted residuals and autocorrelation plots.

Fluorescence intensity decays were analyzed by a sum of discrete exponential terms:[32]

$$I(t) = \sum_{i=1}^{n}\alpha_i\exp(-t/\tau_i) \quad (11)$$

where α_i and τ_i are the pre-exponential term (amplitude) and the lifetime of the ith decay component of fluorescence, respectively. The mean or average fluorescence lifetime is given by:

$$\langle\tau\rangle = \frac{\sum_i \alpha_i\tau_i^2}{\sum_i \alpha_i\tau_i} \quad (12)$$

The fluorescence anisotropy decays, $r(t)$, were analyzed by a sum of discrete exponential terms:[32]

$$r(t) = \sum_{i=1}^{n}\beta_i\exp(-t/\phi_i) + r_\infty \quad (13)$$

where β_i and ϕ_i represent the normalized amplitude and the rotational correlation time of the ith anisotropy decay component, respectively. r_∞ corresponds to the residual or limiting anisotropy, comprising information about the restriction of the depolarizing process.

The wobbling-in-cone model developed by Kinosita and co-workers[34,35] was employed to quantify the extent of restricted motion experienced by TMA-DPH. Briefly, the rotational movement of this fluorescent probe is assumed to be hindered inside a cone-shaped volume with an angle θ_{cone}, which can be deduced from:

https://doi.org/10.1021/acs.langmuir.1c00830
Langmuir 2021, 37, 9952−9963

$$r_\infty/r_0 = \left[\frac{1}{2} \times \cos\theta_{cone} \times (1 + \cos\theta_{cone})\right]^2 \quad (14)$$

where $r_0 = 0.39$[36] is the fundamental anisotropy. The angle θ_{cone} may vary between 0° ($r_\infty = r_0$; fully hindered motion, no rotation) and 90° ($r_\infty = 0$; unhindered motion, complete depolarization). Therefore, a tighter lipid packing in the vicinity of the TMA-DPH probe (larger movement restrictions) should account for a small-angle θ_{cone}.

The rotational diffusion coefficients of TMA-DPH, $D_\perp$, were further determined by:[34,37,38]

$$D_\perp = \frac{0.1674 - 0.1066(r_\infty/r_0) - 0.062(r_\infty/r_0)^2}{\langle\phi\rangle} \quad (15)$$

where $\langle\phi\rangle = \sum_{i=1}^{n} \beta_i\phi_i$ is the average correlation time obtained from the area under the anisotropy decay curve. $D_\perp$ was then converted into an apparent "microviscosity", η, assuming a Brownian diffusion in the framework of the Stokes−Einstein−Debye equation:[39]

$$\eta = \frac{k_B T}{6 D_\perp V_{eff}} \quad (16)$$

where V_{eff} is the effective probe volume. A V_{eff} =360 Å^3 was used considering a polar derivative of DPH,[39] which is structurally similar to the TMA-DPH probe used here.

Laurdan Fluorescence: Generalized Polarization (GP) and Time-Dependent Fluorescence Shift (TDFS) Method. Generalized polarization (GP) of Laurdan, $GP_{Laurdan}$, was calculated from its steady-state emission spectrum according to:[40]

$$GP_{Laurdan} \equiv \frac{I_{440} - I_{490}}{I_{440} + I_{490}} \quad (17)$$

where I_{440} and I_{490} are the fluorescence intensities at 440 and 490 nm, respectively. However, this empirical ratiometric parameter does not allow one to discriminate two effects at the level of lipid interface: (i) the amount of polar solvent molecules (usually water, reporting on surface hydration) and (ii) the local lipid mobility.[41−43]

The time-dependent fluorescence shift (TDFS) method has proved to decipher both effects. Briefly, the fluorescence emission spectra of Laurdan are reconstructed at different times after its excitation, providing insights into the dynamics/evolution toward the final solvent relaxed state (dependent on the local lipid packing (rigidity)), and the final relaxed excited-state energy (proportional to the amount of solvent dipoles (water content)).[32] A detailed theoretical framework was established by Maroncelli and co-workers[44,45] and later applied to model lipid membranes by the group of Hof.[41−43] The primary data consist of the steady-state fluorescence emission spectrum and a series of time-resolved fluorescence intensity decays spanning the emission spectrum of Laurdan (collected between 400 and 540 nm with a 10 nm step). The time-resolved emission spectra, TRES(t), were obtained by the spectral reconstruction method as:[45]

$$TRES(t) \equiv \frac{I_{SS}(\lambda)}{\sum_i \alpha_{i,\lambda}\tau_{i,\lambda}} \sum_i \alpha_{i,\lambda} e^{-t/\tau_{i,\lambda}} \quad (18)$$

where I_{SS} is a normalization factor (from the steady-state emission spectrum), and $\alpha_{i,\lambda}$ and $\tau_{i,\lambda}$ represent the normalized amplitude and the lifetime of the ith decay component of fluorescence for each emission wavelength, respectively. Here, each fluorescence decay was analyzed with four exponential components. TRES(t) values were then expressed in wavenumber units (proportional to energy).[32] Each time point spectrum was fitted with a log-normal function to determine the position of their maxima, ν_p, and the full width at half-maximum, Γ.[45] The overall shift in the emission spectra, $\Delta\nu$, was then calculated as:

$$\Delta\nu = \nu(0) - \nu(\infty) \quad (19)$$

where the position of the TRES maximum at t = 0, $\nu(0)$, was considered as 23,800 cm^{-1},[44] and $\nu(\infty)$ is the maximum position of TRES at the end of relaxation. This spectral shift reflects the degree of solvation (local polarity) at the membrane location of Laurdan. On the other hand, the kinetics of these spectral shifts (relaxation curves) provides information on the reorientation (mobility) of the polar solvent molecules in the immediate vicinity of the probe. Finally, the maximum value of the $\Gamma(t)$ plot (here termed as Γ_{RD}) reports on the heterogeneity of the dipolar relaxation process, i.e., it is informative on the heterogeneity of the solvent shell surrounding each individual fluorophore in the sample. Also, Γ_{RD} is a good estimation of the average time taken by the system to complete the dipolar relaxation process.

RESULTS AND DISCUSSION

SAXS Data of POPC/POPC-OOH Binary Mixtures. The impact of the oxidized lipid POPC-OOH on the structural properties of POPC bilayers was first examined by SAXS. Specifically, the POPC-OOH molar fractions were varied in non-extruded and extruded samples at 23 and 37 °C. Due to the similar features observed from SAXS data at 23 and 37 °C, only data acquired at 23 °C are shown in Figure 2 for simplicity. Data taken at 37 °C are presented in in the Supporting Information (Figure S2).

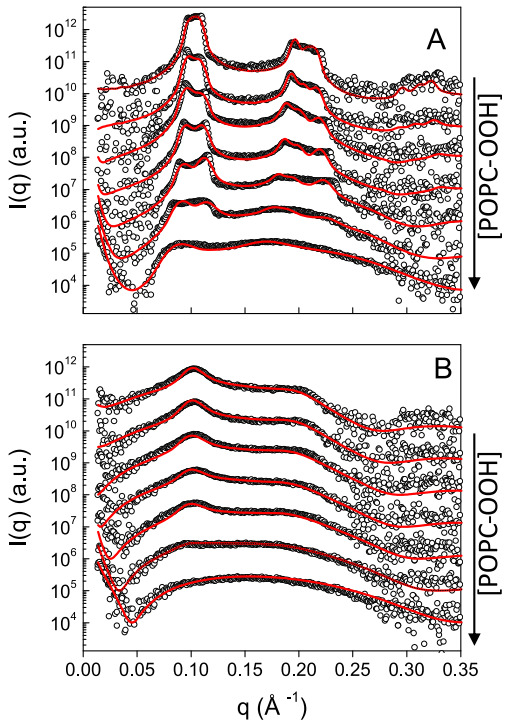

Figure 2. SAXS curves of POPC/POPC-OOHχ with χ = 0, 10, 25, 30, 50, 70, and 100 mol % from top to the bottom (arrow) obtained for (A) non-extruded and (B) extruded samples. Measurements were performed with a total of 10 mM lipid concentration suspended in 10 mM HEPES, 150 mM NaCl, and 0.2 mM EDTA at pH 7.0 measured at 23 °C. The best fit for each experimental curve is depicted in a continuous red line. The fitting parameters are displayed in Table 1. The curves are shifted for better visualization.

A perusal of the SAXS experimental data from non-extruded samples (Figure 2A at 23 °C and Figure S2 at 37 °C) evidences diffraction peaks (first order and second order, see below) due to the lipid bilayer stacking of MLVs in solution. The positions of such diffraction peaks are practically the same at both temperatures (Figure S2), evidencing that the interbilayer distance did not change within this temperature interval. An intensity decrease was thoroughly observed by

https://doi.org/10.1021/acs.langmuir.1c00830
Langmuir 2021, 37, 9952−9963

Table 1. Parameters Obtained from the Fittings of Lipid Bilayer Cross-Sectional $P_t(q)$ Form Factors (eqs 2−4) to the Experimental SAXS Data of Extruded and Non-extruded Samples (Figure 2) at 23 °C, Both through a Global Fitting Procedure[a]

POPC/POPC-OOH	100:0	90:10	75:25	70:30	50:50	30:70	0:100
			$P_t(q)$ modeling				
R_{pol} (Å)	9.9(6)	9.9(4)	9.8(7)	9.9(6)	9.9(4)	10.0(3)	10.0(4)
R_{CH2} (Å)	10.7(5)	10.3(5)	9.7(6)	9.5(5)	8.7(5)	7.9(4)	6.7(6)
R_{CH3} (Å)	2.7(5)	2.7(5)	2.7(6)	2.7(5)	2.7(4)	2.7(4)	2.7(5)
ρ_{pol} (e Å^{-3})	0.451(8)	0.451(6)	0.454(8)	0.455(7)	0.458(4)	0.460(6)	0.465(9)
ρ_{CH2} (e Å^{-3})	0.329(8)	0.328(9)	0.327(8)	0.327(8)	0.324(6)	0.322(5)	0.320(8)
ρ_{CH3} (e Å^{-3})	0.202(4)	0.202(4)	0.202(3)	0.202(3)	0.202(3)	0.202(3)	0.202(4)
			$S(q)$ extruded vesicles				
γ	0.47(2)	0.42(2)	0.46(2)	0.57(2)	0.54(2)	0.83(2)	0.99(2)
N	6(2)	6(2)	5(2)	5(2)	5(2)	4(2)	2(2)
D_{rep} (Å)	61(3)	62(2)	62(2)	62(2)	63(2)	63(2)	64(2)
			$S(q)$ MLVs				
N	10(2)	9(2)	8(2)	8(2)	7(2)	5(2)	3(2)
$\langle D_{rep} \rangle$ (Å)	60(2)	61(3)	62(3)	62(3)	63(4)	64(4)	71(5)
$\eta_{Caillé}$	0.04(1)	0.05(1)	0.07(1)	0.08(1)	0.10(1)	0.12(1)	0.15(1)

[a]Electron density and thickness for the each region: polar headgroup (ρ_{pol}, R_{pol}), paraffinic chains (ρ_{CH2}, R_{CH2}), and methyl group (ρ_{CH3}, R_{CH3}); γ (eq 4) means the fraction of LUVs in each sample of extruded vesicles. $S(q)$ parameters, N (number of stacked bilayers), D_{rep} (interbilayer repetition distance), and $\eta_{Caillé}$ (Caillé parameter) (eqs 5 and 8), were obtained via the modified Caillé theory; for MLVs, $\langle D_{rep} \rangle$ values are averaged values (see Experimental Section for details). The numbers in parentheses mean parameter uncertainties.

raising the temperature from 23 °C to 37 °C (Figure S2). Noteworthily, the diffraction peak intensities were significantly more affected by increasing the amount of POPC-OOH in the membrane rather than by increasing the temperature (Figure 2A and Figure S2). Indeed, SAXS data for membranes with the POPC-OOH content greater than 50 mol % are identical independent of temperature (Figure S2). Such a finding points out that the presence of this hydroperoxidized lipid in the membrane destabilizes the bilayer stacking to a larger extent than does the temperature variation from 23 to 37 °C. Upon extrusion, a large number of the MLVs are disrupted and LUVs are predominant as one can observe from less pronounced diffraction peaks from SAXS data without any temperature influence within the investigated interval (Figure 2B at 23 °C and Figure S2 at 37 °C). MLVs practically disappear upon increasing the POPC-OOH amount into the extruded vesicles.

To better describe the bilayer features upon increasing the oxidized lipid molar fraction as well as how POPC-OOH impacts the bilayer stacking, SAXS data were thus analyzed by the modified Caillé theory (MCT). Figure 2 presents the best fittings (solid lines) to the experimental data, whereas the fitting parameters are presented in Table 1. As one can see, there is very good agreement between the modeling and the experimental SAXS curves for all POPC/POPC-OOH mixtures for extruded and non-extruded samples. From the fitting parameters related to the bilayer cross-sectional form factor $P_t(q)$ (eqs 2 and 3), the corresponding electron density profiles were calculated and are depicted in Figure 3. Interestingly, the lipid bilayer thickness decreases upon increasing the POPC-OOH amount in the membrane, as previously reported for POPC/POPC-OOH mixtures dispersed in Milli-Q water[12] also analyzed by SAXS through the scattering density profile modeling. Furthermore, the presence of POPC-OOH increases the electron density around 10 Å from the center of the lipid bilayer (Figure 3), which can be

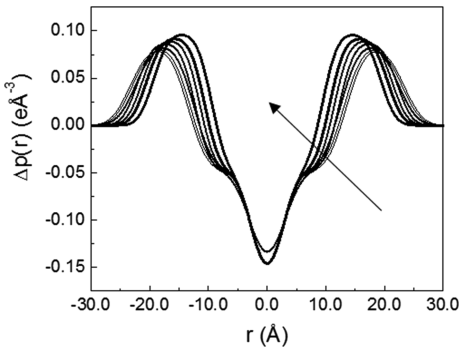

Figure 3. Electron density profile $\Delta\rho(r) = \rho(r) - \rho_{buf}$ calculated using the $P_t(q)$ parameters obtained through the fittings to the experimental SAXS curves for each POPC/POPC-OOHχ composition with χ = 0, 10, 25, 30, 50, 70, and 100 mol % (arrow direction).

attributed to the preferential position of the hydroperoxide group in the apolar/polar membrane interface.[11−13] According to previous works, the presence of the OOH group in the membrane interface promotes an increase in the membrane surface area,[11−13] with a higher hydration of the membrane.[12,13]

The temperature increase from 23 °C to 37 °C did not impact the structure of the membrane, $P(q)$, for any lipid composition. This is probably due to the fact that all POPC/POPC-OOH mixtures are already in the fluid phase at 23 °C, and thus, no significant alteration was observed by means of SAXS. For example, between 20 and 40 °C, the POPC membrane's thickness and area per lipid decrease only by 1 Å and 1.5 Å^2, respectively.[46]

As mentioned above, SAXS curves obtained from non-extruded and extruded POPC samples (Figure 2) display diffraction peaks, implying lipid bilayer stacking. For MLVs (Figure 2A), the observable peaks are split in three interference

https://doi.org/10.1021/acs.langmuir.1c00830
Langmuir 2021, 37, 9952−9963

functions ($S(q)$) (see Figure S1) due to the influence in the membrane of the saline-buffered solution as previously reported for phosphatidylcholine membranes.[31] Of note, for extruded samples, there is a fraction of MLVs with a few stacked bilayers ($N = 4–6$) with $D_{rep} = 62(1)$ Å coexisting with LUVs (Figure 2B and Table 1). Such a contribution decreases with the POPC-OOH percentage, amounting to circa 50% for pure POPC membranes until the abolishment of bilayer stacking for extruded vesicles composed of 100 mol % POPC-OOH (Figure 2B and Table 1). Moreover, the number N of stacked bilayers decreases for an increasing number of oxidized lipids in POPC MLVs (Table 1) with concomitant swelling in-between bilayers. Indeed, the hydration layer thickness, d_w ($d_w = D_{rep} - (2 \times (R_{CH3} + R_{CH2} + R_{pol}))$), increases from 13.4 ± 2.2 Å for POPC MLVs to 32 ± 5 Å for POPC-OOH MLVs (Table 1 and Figure 4A). The values of POPC bilayer

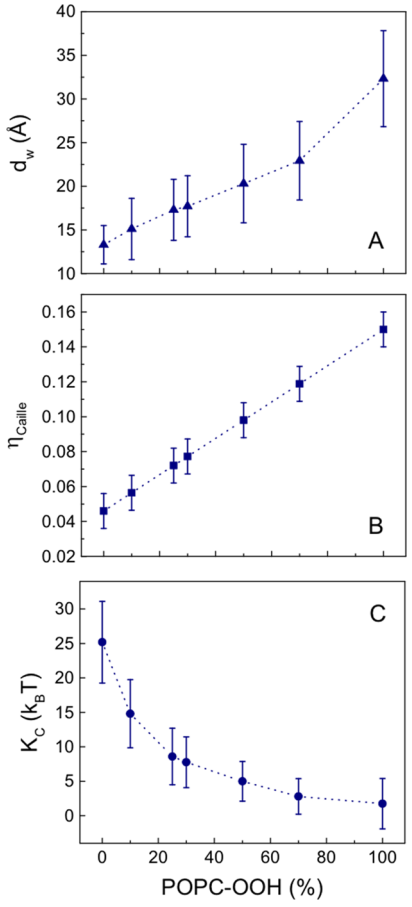

Figure 4. (A) Hydration layer thickness, $d_w = (D_{rep} - 2 \times (R_{CH3} + R_{CH2} + R_{pol}))$ as a function of the increase in the molar percentage of POPC-OOH in POPC MLVs, (B) $\eta_{Caillé}$ parameter values obtained from $S(q)$ functions fitting to SAXS data at 23 °C, and (C) corresponding values of the bending modulus, K_c, calculated by using eq 8. Averaged values of D_{rep} are shown in Table 1. Dotted lines are drawn just as a guide to the eye.

thickness and hydration layer here evaluated are in very good agreement with those previously reported for POPC MLVs in the presence of 150 mM NaCl.[47] On the other hand, to the best of our knowledge, this is the first report demonstrating significant swelling in-between hydroperoxidized bilayers in respect to non-oxidized ones.

Therefore, the presence of POPC-OOH lipids in the membrane seems to hinder bilayer stacking and is accompanied by a significant increase in the interbilayer water thickness d_w. To better understand such an effect, the values of bending modulus K_c were also determined (eq 8), where the Caillé parameters (Table 1) and D_{rep} values were obtained through $S(q)$ fittings to the experimental curves (Table 1) and the bulk modulus of compression was assumed as $B = 15 \times 10^{12}$ erg cm^{-4}.[48] Values of $\eta_{Caillé}$ and K_c at 23 °C upon increasing the POPC-OOH molar fraction are presented in Figure 4B,C, respectively.

Noteworthily, the averaged $\eta_{Caillé}$ (Figure 4B) increased from about 0.04(1) for POPC to 0.15(1) for POPC-OOH membranes. The $\eta_{Caillé}$ value obtained here for POPC at 23 °C is in good agreement with that previously reported for the POPC MLVs at 25 °C.[47] Further, such a rise in $\eta_{Caillé}$ for hydroperoxide-containing membranes implies an increase in bending fluctuations, which decreases the positional correlations. In turn, the lipid bilayer bending rigidity K_c decreases circa 10-fold from pure POPC membranes to pure POPC-OOH membranes. The K_c value of 25 k_BT for the POPC membrane here determined by X-ray diffraction is in good agreement with the value reported by Bouvrais et al.,[49] who evaluated membrane fluctuations of POPC GUVs dispersed in a similar buffer solution. To date, this is the first report on membrane bending rigidity K_c values for membranes containing binary mixtures of POPC/POPC-OOH as well as pure hydroperoxide POPC lipid. A decrease in bending modulus has already been predicted from MD simulations for oxidized truncated lipids.[50] Enhanced membrane undulations were previously observed in POPC-OOH GUVs.[4,17] Here, our experimental approach allowed us to quantify changes in K_c values for partially and fully hydroperoxidized lipid bilayers, which account for the observed swelling in-between the oxidized bilayers. It should be remarked that anomalous swelling has been previously observed for dimyristoylphosphatidylcholine (DMPC) stacked bilayers near its phase transition associated with the decrease in membrane bending rigidity, with no changes in van der Waals or hydration forces.[48] Of note, K_c values for hydroperoxidized lipid membranes are on the same order of those previously reported for surfactant microemulsion[51] and surfactant monolayers,[52] also indicating the high flexibility of such an oxidized membrane.

Last, upon comparing the results obtained at 23 and 37 °C, the most significant difference is the less intense second-order peak of the interference function for the non-extruded samples at 37 °C (Figure S2). Moreover, the difference of the intensities of the diffraction peaks decreases with the increase in POPC-OOH molar fraction, and for 70 and 100% POPC-OOH, no distinction is observed for both temperatures (Figure S2). These results are compatible with the following: (i) the increase in temperature promotes membrane fluctuations (increasing the $\eta_{Caillé}$), thus decreasing the peak intensity, and (ii) the fluctuation in the membrane rises with the increase in POPC-OOH molar fraction, and for 70 and 100% oxidized lipid, the level of fluctuations is already at such a high level that the increase in temperature does not impact this parameter any further.

To better understand why the hydroperoxide lipid imparts a decrease in the bending rigidity, further steady-state and time-resolved fluorescence experiments were performed using two fluorescent extrinsic probes, TMA-DPH and Laurdan, as

https://doi.org/10.1021/acs.langmuir.1c00830
Langmuir 2021, 37, 9952−9963

follows to obtain information on the membrane interfacial properties (including order, microviscosity, and hydration).

Interfacial Membrane Characterization of POPC/POPC-OOH Binary Mixtures from Fluorescence Spectroscopy. We next sought to investigate the effects of the oxidized lipid POPC-OOH on fluid POPC bilayers at the level of the lipid/water interface. Steady-state and time-resolved fluorescence measurements of TMA-DPH were carried out for various MLV POPC/POPC-OOH binary mixtures again at 23 and 37 °C. This well-established fluorescent probe is anchored at the membrane interface by its polar trimethylammonium group. Therefore, it is expected to be a good reporter of the interfacial perturbations induced by the hydroperoxide group of POPC-OOH, which is preferentially localized at this membrane region as indicated by SAXS (Figure 3). Specifically, the center of mass of TMA-DPH is around 10 Å in POPC membranes,[53] in close vicinity to the position of the −OOH moiety, about 7−10 Å from the center of the membrane (Figure 3).[12] The precise location of TMA-DPH in POPC-OOH membranes may be slightly changed. However, a similar localization can still be expected, since the polar trimethylammonium group should always anchor the TMA-DPH probe at the interface.

Figure 5A shows the variation of the mean fluorescence lifetime of TMA-DPH, $\langle\tau\rangle_{TMA-DPH}$, in POPC membranes prepared with increasing amounts of POPC-OOH (ranging from χ = 0 to 100%). We note that in case that phase separation happens in this lipid binary system, the close-to-linear variation of $\langle\tau\rangle_{TMA-DPH}$ with the POPC-OOH molar fraction points out to a partition coefficient of the TMA-DPH probe between these putative phases close to unity, which is expected considering that both phases are fluid. In this case, the probe would report global information about the whole membrane alteration. The $\langle\tau\rangle_{TMA-DPH}$ values obtained for pure POPC membranes again are in agreement with earlier studies ($\langle\tau\rangle$= 4.2 ns at 23 °C[21,54,55] and 3.0 ns at 37 °C[56]). Remarkably, $\langle\tau\rangle_{TMA-DPH}$ strongly decreases with the POPC-OOH molar fraction in the membrane, particularly at 23 °C (4.2 to 3.4 ns from 0 to 100 mol % POPC-OOH) (Figure 5A). These results reveal that TMA-DPH senses a higher water content in its vicinity in the presence of the oxidized lipid POPC-OOH, i.e., the membrane interface becomes progressively more hydrated upon increasing the mol % of the oxidized lipid. In addition, the OOH groups might be also quenching the fluorescence emitted by TMA-DPH. Considering that the water molecules are the major collisional quenchers of TMA-DPH,[57] the variation of $\langle\tau\rangle_{TMA-DPH}$ can be used to estimate a majorant of the increase in membrane surface hydration. Considering a ratio of Stern−Volmer relationships in the transient state (no static quenching)[57] and the fluorescence lifetime of DPH (as a reference), in the absence of a quencher (in an apolar viscous isotropic solvent, here used 13.2 ns in dodecane at 23 °C[58]), an increase in water content up to 54% is predicted for pure POPC-OOH as compared to pure POPC membranes at 23 °C. It should be stressed that the concomitant changes in membrane viscosity revealed by the time-resolved anisotropy measurements (discussed later in the text (Figure 6C)) have been taken into account in these calculations via Smoluchowski[32] and Stokes−Einstein equations (eq 16). Previous SAXS data analysis pointed out an increase from about 23 to 35 water molecules in the lipid bilayer when POPC is replaced by POPC-OOH, which represents an ∼52% increase in water content,[12] showing good agreement between the values obtained using two independent methodologies. The small difference can eventually be attributed to the participation of the OOH group in the fluorescence quenching process of TMA-DPH as mentioned above. In addition, applying a similar approach to the lifetime data obtained at 37 °C (Figure 5A), a very similar increase in water content of 59% is obtained, revealing the steric perturbation introduced by the OOH group at the membrane interface.

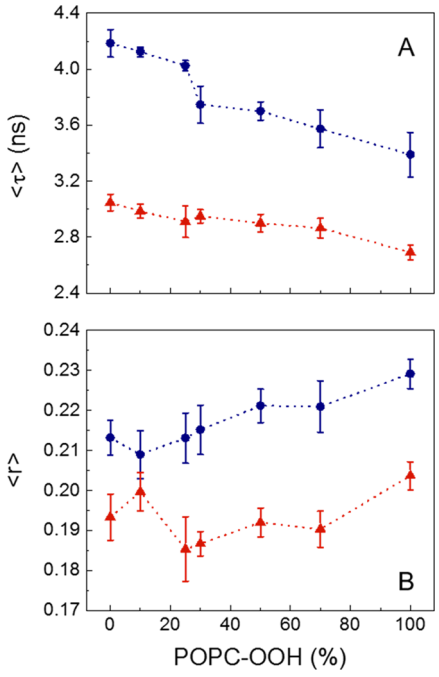

Figure 5. Variation of (A) the average fluorescence lifetime $\langle\tau\rangle$ and (B) the steady-state fluorescence anisotropy $\langle r\rangle$ of TMA-DPH with the POPC-OOH molar fraction at 23 °C (blue circles) and 37 °C (red triangles). TMA-DPH was incorporated in 0.1 mM POPC:-POPC-OOH MLVs at a 1:200 probe:lipid ratio. Lines are drawn as guides to the eye. Values are the averages (±SD) of at least three independent experiments.

To gain further information about the influence of POPC-OOH on the interfacial lipid packing, steady-state fluorescence anisotropy measurements were also performed for TMA-DPH, $\langle r\rangle_{TMA-DPH}$, at the two temperatures. $\langle r\rangle_{TMA-DPH}$ values obtained here for pure POPC at both temperatures are identical to the ones previously reported (0.21 and 0.19 at 23 and 37 °C, respectively).[21] This parameter displays a slight increase with the mol % of POPC-OOH, particularly at 23 °C (Figure 5B). However, these changes in $\langle r\rangle_{TMA-DPH}$ do not directly imply that the membrane is becoming more rigid/ordered in the presence of POPC-OOH, since an increase in this parameter can be produced by a concomitant shortening of $\langle\tau\rangle_{TMA-DPH}$ (from the Perrin equation[32]), as shown in Figure 5A. To distinguish both effects, i.e., an increase in water content (shorter $\langle\tau\rangle_{TMA-DPH}$) and/or in the rigidity/order at the membrane interface, time-resolved fluorescence anisotropy experiments were also performed for TMA-DPH in POPC/POPC-OOH binary mixtures.

Fluorescence anisotropy decays of TMA-DPH for different POPC/POPC-OOH binary mixtures at 23 and 37 °C are shown in Figure S3, displaying in all cases a limiting anisotropy. These decays were adequately fitted by a sum of

https://doi.org/10.1021/acs.langmuir.1c00830
Langmuir 2021, 37, 9952−9963

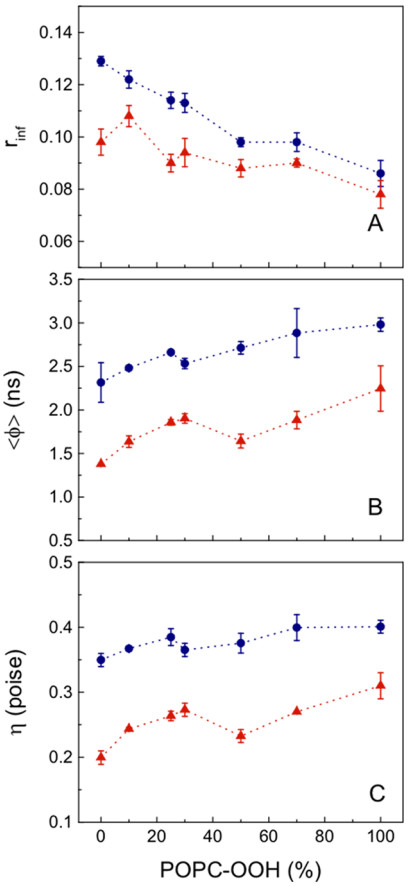

Figure 6. Dependence of (A) the residual anisotropy r_∞, (B) the average rotational correlation time $\langle\phi\rangle$ of TMA-DPH, and (C) the computed membrane viscosity η with the POPC-OOH molar fraction at 23 °C (blue circles) and 37 °C (red triangles). The first two parameters were determined from time-resolved anisotropy decays of TMA-DPH and η was calculated using eq 16. The probe was loaded in 0.1 mM POPC:POPC-OOH MLVs at a 1:200 probe:lipid ratio. Lines are just a guide to the eye. Values are the averages (±SD) of at least three independent measurements.

two exponential terms plus a limiting anisotropy at both temperatures (eq 13) (Table S1). The variations of the limiting anisotropy, $r_{\infty \mathrm{TMA-DPH}}$, and the average rotational correlation time of TMA-DPH, $\langle\phi\rangle_{\mathrm{TMA-DPH}}$, at 23 and 37 °C are plotted as a function of POPC-OOH content (mol %) in POPC membranes in Figure 6A,B. The recovered parameters are in general agreement with data obtained for TMA-DPH in pure POPC membranes at similar temperatures.[59]

$r_{\infty \mathrm{TMA-DPH}}$ progressively decreases from 0.13 to 0.09 from 0 to 100% POPC-OOH at 23 °C, whereas a smaller variation is observed at 37 °C (Figure 6A). Again, the intrinsic membrane dynamics at 37 °C is already high, and $r_{\infty \mathrm{TMA-DPH}}$ is less affected by the OOH group at this temperature. These results reveal that POPC-OOH reduces the membrane order at 23 °C, i.e., the hydroperoxide group compromises the membrane structure of POPC membranes at this temperature and so enables slightly larger wobbling-in-cone fluctuations for TMA-DPH. Considering the wobbling-in-cone model of Kinosita et al.,[34,35] this leads to angles of θ_{cone} = 47° and 54° for pure POPC and POPC-OOH, respectively (eq 14).

Concomitantly, $\langle\phi\rangle_{\mathrm{TMA-DPH}}$ presents a moderate increasing trend with the POPC-OOH content in fluid POPC membranes at both temperatures (from 2.3 to 3.0 ns at 23 °C and 1.4 to 2.2 ns at 37 °C, from 0 up to 100% POPC-OOH) (Figure 6B). We further determined the rotational diffusion coefficient perpendicular to the z-axis of TMA-DPH, $D_\perp$ (eq 15), since this is the most relevant mechanism contributing to the fluorescence depolarization of this membrane probe. The microviscosity near TMA-DPH, $\eta_{\mathrm{TMA-DPH}}$, was then obtained from eq 16. Figure 6C shows that this fluorescent probe is sensing a slightly higher microviscosity at the lipid/water interface for the oxidized POPC membranes compared to pure POPC membranes. This result agrees with a recent fluorescence-lifetime imaging microscopy (FLIM) study of GUVs using a molecular rotor to determine changes in viscosity upon oxidation of the lipid 1,2-dioleoyl-*sn*-glycero-3-phosphocholine (DOPC).[60] In the case of type II photooxidation, where precisely the same type of oxidized lipid is obtained (insertion of a −OOH group near the double bond such as in our work), the authors also observed an increase in viscosity, in this case, in a more hydrophobic region of the membrane. It should be stressed that the simultaneous decrease in membrane order and the local increase in microviscosity are an unusual trend, as, e.g., in the membrane phase transition from gel to fluid, both the membrane microviscosity and lipid order decrease simultaneously.[32] Therefore, our results indicate that the perturbation induced by the oxidized moiety may turn the membrane simultaneously less ordered and more viscous.

We further explored the perturbations introduced by the hydroperoxide group in fluid POPC membranes at the level of lipid carbonyls by Laurdan fluorescence. We initially addressed it from the usual GP parameter (eq 17) for this solvatochromic probe (Figure 7A), which globally evaluates the efficiency of the probe excited-state relaxation process due to its environment. Our results show that $\mathrm{GP_{Laurdan}}$ smoothly increases with the POPC-OOH molar fraction at 23 °C to a higher plateau value ($\mathrm{GP_{Laurdan}} \approx -0.12$), whereas this effect is more noticeable at 37 °C. Of note, the $\mathrm{GP_{Laurdan}}$ values obtained here for 100 mol % POPC at both 23 and 37 °C are in good agreement with data previously reported in the literature.[43] However, this steady-state approach cannot separate two effects: changes in (i) local polarity (hydration level) and (ii) the dynamics of solvent dipole reorientation upon probe excitation, which is controlled by the local lipid packing. For this purpose, we employed the TDFS method to Laurdan in 100 mol % POPC or POPC-OOH membranes (Figure 7B−D). From the TRES analysis, the maximum wavenumber and the full width at half-maximum (ν_p and Γ, respectively) for each spectrum of Laurdan at several times after its excitation were determined, and their time evolution is shown in Figure 7C,D.

Figure 7C shows both the dynamics of the relaxation process and the limiting energy value of the red-shifted emission of Laurdan, $\nu(\infty)$. This last parameter allows one to estimate the extent of energy stabilization, $\Delta\nu$ (eq 19), which is proportional to the number of solvent dipoles involved in the relaxation process. For pure POPC, $\Delta\nu$ is about 4080 $\mathrm{cm^{-1}}$ at both temperatures, at variance with the observation for the oxidized lipid POPC-OOH. In addition, the average relaxation time of the probe was determined from the time where $\Gamma(t)$ reaches its maximum, Γ_{RD} (Figure 7D). For POPC membranes at 23 and 37 °C, the values are 1.08(6) and 0.39(6) ns, respectively. These values are again in good agreement with the published data.[43]

https://doi.org/10.1021/acs.langmuir.1c00830
Langmuir 2021, 37, 9952−9963

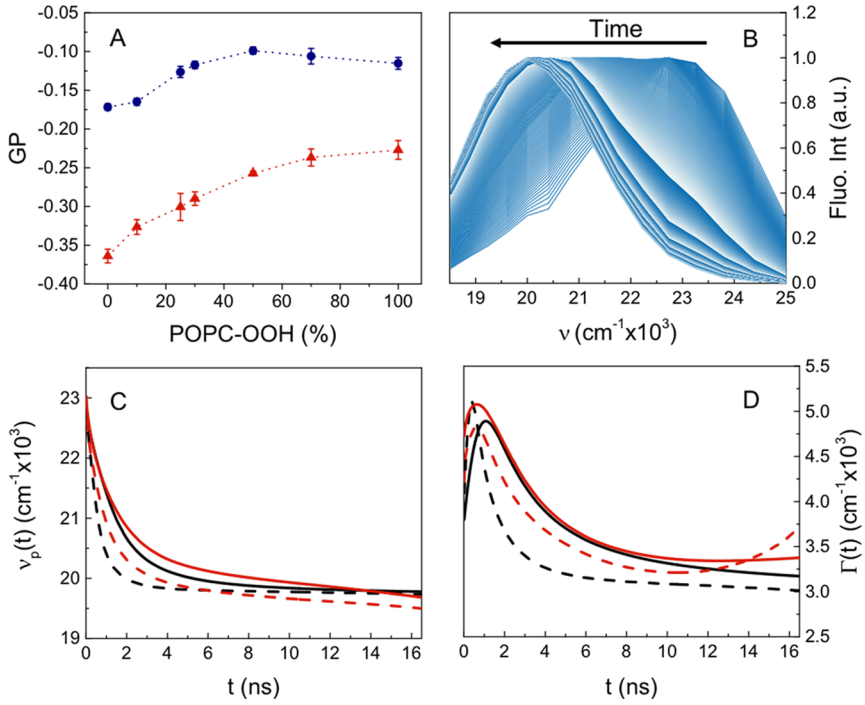

Figure 7. Fluorescence solvent relaxation parameters for Laurdan in POPC-OOH membranes. (A) Changes in generalized polarization (GP) of Laurdan as a function of the POPC-OOH molar fraction at 23 °C (blue circles) and 37 °C (red triangles). Lines are drawn just as a guide to the eye. Values are the averages (±SD) of at least three independent experiments. (B) TRES of Laurdan in pure POPC-OOH LUVs. The figure shows 1390 spectra in steps of 0.015 ns between t = 0.015 ns and t = 20.85 ns. (C) Time dependence of the peak maximum position ν_p and (D) the full-width at half-maximum Γ of TRES of Laurdan in pure POPC (black) or POPC-OOH (red) LUVs at 23 °C (solid line) and 37 °C (dashed line). In all measurements, Laurdan was incorporated in 0.5 mM POPC:POPC-OOH LUVs at a 1:100 probe:lipid ratio.

For POPC-OOH membranes, although the relaxation process appears to be not yet finalized within the operational time window allowed for the experiment (16 ns, see Figure 7C,D), the relaxation kinetics is clearly slower for this oxidized lipid compared to POPC membranes at both temperatures. This supports the conclusion that the reorientation of the water dipoles around the excited state of Laurdan is slowed down in this membrane environment as the interface becomes more packed due to the presence of the OOH groups (in agreement with the time-resolved fluorescence anisotropy data, Figure 6C). Particularly at 37 °C, the extent of the relaxation is greater for POPC-OOH (lower $\nu(\infty)$) as compared to POPC membranes, indicating that more solvent dipoles (water) are present at the membrane interface (as expected from the shorter $\langle\tau\rangle_{TMA-DPH}$ in POPC-OOH membranes, Figure 5A).

In addition, $\Gamma(t)$ displays a complex behavior for the POPC-OOH lipid. First, Γ_{RD} is attained at shorter times for POPC-OOH compared with POPC at 23 °C, reporting that the maximum heterogeneity of solvated states happens at the beginning of the relaxation process. Interestingly, Γ increases significantly at times longer than 10 ns, which means that a complex relaxation process is dominant in this time window. This effect is more noticeable at 37 °C. At variance for POPC, the relaxation dynamics is almost completed by that time.

Altogether, TRES analysis reveals, for the oxidized lipid POPC-OOH, (i) an increase in the dipolar relaxation time and (ii) a concomitant increase in the number of dipoles interacting with Laurdan ($\Delta\nu$), implying a higher hydration of the membrane. Certainly, both physical properties should account for distinct effects on $GP_{Laurdan}$. Thus, the increase in the dipolar relaxation time plays the largest impact on $GP_{Laurdan}$, leading globally to its increase. However, although the incorporation of other oxidized truncated lipids (such as PazePC and PoxnoPC) in POPC membranes also results in the increase in hydration as here observed for the POPC-OOH lipid, their mobility (smaller viscosity) also increases,[61] at variance with our observation for POPC-OOH with two long aliphatic chains. A similar effect to the POPC-OOH lipid was previously reported for POPC membranes in the presence of oxeprenolol and propranolol,[62] in which the increase in $GP_{Laurdan}$ is given by (i) the increase in the dipolar relaxation time (increases GP) and (ii) the increase in the hydration (higher $\Delta\nu$ decreases GP).

Finally, the complex relaxation process observed for Laurdan in the presence of POPC-OOH may be explained by the hydroperoxide group localized at the same membrane region of the probe as indicated by SAXS (Figure 3).[12] In fact, TRES analysis for POPC membranes (at 37 °C) with different oxidized cholesterols containing the OH group already reported that $\nu_p(t)$ did not reach a plateau in the experiment timescale (such as here observed in Figure 7D for the POPC-OOH lipid). In addition, the appearance of more than one peak in $\Gamma(t)$ was reported.[63] However, this complex dipolar relaxation process for Laurdan was not observed in the presence of other oxidized cholesterols without the OH group.[63] Therefore, this suggests that both the OH group of water[63] and the OOH group of the oxidized lipid (when present in the same bilayer region of Laurdan) contribute to the probe relaxation process. Expectedly, the OOH group can interact with Laurdan, since it is located about 7−10 Å from the center of the bilayer,[12,13] near the fluorescent probe around 11.4 Å in DOPC membranes.[64] Although the exact position of Laurdan might change, this probe has a well-defined membrane location in the bilayer at the carbonyl level.

https://doi.org/10.1021/acs.langmuir.1c00830
Langmuir 2021, 37, 9952−9963

CONCLUSIONS

Our combined SAXS and time-resolved fluorescence methodologies provided a detailed understanding of the structural and dynamic perturbations introduced by the oxidized lipid POPC-OOH in fluid POPC lipid bilayers. Specifically, SAXS experiments probed alterations at the macroscopic level of the hydroperoxide-containing membranes, whereas fluorescence measurements of Laurdan/TMA-DPH mapped the local changes at the lipid/water interface.

SAXS data show that the incorporation of the oxidized lipid POPC-OOH decreases the lipid bilayer thickness, in which the −OOH group preferentially localizes ∼10 Å from the center of the lipid bilayer (at the apolar/polar membrane interface) in agreement with a previous work.[12] In addition, the data reveal that the −OOH group disorganizes the membrane structure, which results in the decrease in the membrane bending modulus (here observed from SAXS) and the decrease in the stretching modulus as reported by Weber et al.[11] Such an in-plane membrane order decrease must also hinder the correlation between bilayers that, associated with enhanced membrane fluctuations, disfavors bilayer stacking as shown by the disappearance of Bragg peaks in SAXS data (Figure 2 and Table 1) obtained for POPC-OOH extruded vesicles. A concomitant significant swelling in-between POPC/POPC-OOH stacked bilayers takes place as the oxidized lipid amount increases in the lipid membrane.

The time-resolved fluorescence experiments of TMA-DPH and the TDFS of Laurdan explored the membrane interfacial properties of POPC-OOH-containing membranes, including the order, viscosity, and hydration. Both Laurdan and TMA-DPH report that the oxidized lipid moiety increases the membrane hydration near the apolar/polar interface (lower $\langle\tau\rangle_{TMA-DPH}$ and $\nu(\infty)$ for POPC-OOH membranes) (Figures 5A and 7C). Strikingly, Laurdan presents a complex and slower relaxation process in the presence of the −OOH group (Figure 7C,D), supporting a higher lipid packing at the oxidized membrane interface. In addition, the microviscosity near TMA-DPH also slightly increases for enriched POPC-OOH membranes. This is likely due to the high molecular density at the probe region as revealed by SAXS (Figure 3), since the −OOH group localizes at a similar lipid bilayer position as the one of Laurdan and TMA-DPH, and also to the existence of an efficient hydrogen bond network, involving the −OOH groups near the surface.[65] Simultaneously, the decrease in the limiting anisotropy of TMA-DPH with the POPC-OOH amount indicates a decrease in membrane order. This clearly shows that the membrane structure, at least near the interface, is compromised, in line with SAXS data. In addition, at variance with the usual observation for membrane fluidization upon the introduction of membrane perturbations, in this case, the membrane becomes more viscous.

SAXS data also reveal that the membrane perturbation for high molar fractions of POPC-OOH is already so strong at 23 °C that an increase in temperature to 37 °C does not significantly impact the retrieved parameters regarding membrane fluctuations. Finally, the decrease in the elastic moduli of the membranes due to hydroperoxide lipids leads to membrane remodeling.[4]

ASSOCIATED CONTENT

Supporting Information

The Supporting Information is available free of charge at https://pubs.acs.org/doi/10.1021/acs.langmuir.1c00830.

Typical analysis of an SAXS experimental curve for non-extruded POPC at 23 °C (Figure S1); SAXS data at 37 °C for extruded and non-extruded vesicles (Figure S2); time-resolved fluorescence anisotropy decays (Figure S3); fluorescence parameters determined for TMA-DPH (Table S1) (PDF)

AUTHOR INFORMATION

Corresponding Authors

Ana M. Melo − *iBB−Institute for Bioengineering and Biosciences, Instituto Superior Técnico, Universidade de Lisboa, Lisboa 1049-001, Portugal; Associate Laboratory i4HB−Institute for Health and Bioeconomy at Instituto Superior Técnico, Universidade de Lisboa, Lisboa 1049-001, Portugal;* orcid.org/0000-0002-2086-5939; Email: anammelo@tecnico.ulisboa.pt

Rosangela Itri − *Institute of Physics, University of São Paulo, São Paulo 05508-090, Brazil;* orcid.org/0000-0001-9311-0804; Email: itri@if.usp.br

Authors

Gustavo Scanavachi − *Institute of Physics, University of São Paulo, São Paulo 05508-090, Brazil;* Present Address: Department of Cell Biology, Harvard Medical School, Boston, Massachusetts 02115, United States; Program in Cellular and Molecular Medicine, Boston Children's Hospital, Boston, Massachusetts 02115, United States

Ana Coutinho − *iBB−Institute for Bioengineering and Biosciences, Instituto Superior Técnico, Universidade de Lisboa, Lisboa 1049-001, Portugal; Associate Laboratory i4HB−Institute for Health and Bioeconomy at Instituto Superior Técnico, Universidade de Lisboa, Lisboa 1049-001, Portugal; Dep. Química e Bioquímica, Faculdade de Ciências, Universidade de Lisboa, Lisboa 1749-016, Portugal;* orcid.org/0000-0003-1653-0703

Alexander Andreevich Fedorov − *iBB−Institute for Bioengineering and Biosciences, Instituto Superior Técnico, Universidade de Lisboa, Lisboa 1049-001, Portugal; Associate Laboratory i4HB−Institute for Health and Bioeconomy at Instituto Superior Técnico, Universidade de Lisboa, Lisboa 1049-001, Portugal*

Manuel Prieto − *iBB−Institute for Bioengineering and Biosciences, Instituto Superior Técnico, Universidade de Lisboa, Lisboa 1049-001, Portugal; Associate Laboratory i4HB−Institute for Health and Bioeconomy at Instituto Superior Técnico, Universidade de Lisboa, Lisboa 1049-001, Portugal*

Complete contact information is available at: https://pubs.acs.org/10.1021/acs.langmuir.1c00830

Notes

The authors declare no competing financial interest.

ACKNOWLEDGMENTS

The authors acknowledge funding from São Paulo Research Foundation (FAPESP, 2014/20107-7) and Fundação para a Ciência e a Tecnologia, Portugal (FCT projects: FAPESP/

20107/2014, PTDC/BTM-SAL/31057/2017, PTDC/BIA-BFS/30959/2017, and UIDB/04565/2020). R.I. is a recipient of CNPq research fellowship. A.A.F. acknowledges a research contract (IST-ID/105/2018). A.M.M. is a Junior Researcher under the FCT CEEC−Individual Call (CEECIND/00884/2017). G.S. acknowledges PhD scholarship from the Coordination for the Improvement of Higher Education Personnel (CAPES) and its Science without Borders Program.

REFERENCES

(1) Yin, H.; Xu, L.; Porter, N. A. Free radical lipid peroxidation: mechanisms and analysis. *Chem. Rev.* **2011**, *111*, 5944−5972.
(2) Niki, E. Lipid peroxidation: Physiological levels and dual biological effects. *Free Radical Biol. Med.* **2009**, *47*, 469−484.
(3) Girotti, A. W.; Korytowski, W. Cholesterol Peroxidation as a Special Type of Lipid Oxidation in Photodynamic Systems. *Photochem. Photobiol.* **2019**, *95*, 73−82.
(4) Tsubone, T. M.; Baptista, M. S.; Itri, R. Understanding membrane remodelling initiated by photosensitized lipid oxidation. *Biophys. Chem.* **2019**, *254*, 106263.
(5) Tsubone, T. M.; Junqueira, H. C.; Baptista, M. S.; Itri, R. Contrasting roles of oxidized lipids in modulating membrane microdomains. *Biochim. Biophys. Acta* **2019**, *1861*, 660−669.
(6) Dos Santos, A. F.; Inague, A.; Arini, G. S.; Terra, L. F.; Wailemann, R. A. M.; Pimentel, A. C.; Yoshinaga, M. Y.; Silva, R. R.; Severino, D.; de Almeida, D. R. Q.; Gomes, V. M.; Bruni-Cardoso, A.; Terra, W. R.; Miyamoto, S.; Baptista, M. S.; Labriola, L. Distinct photo-oxidation-induced cell death pathways lead to selective killing of human breast cancer cells. *Cell Death Dis.* **2020**, *11*, 1070.
(7) Reis, A. Oxidative Phospholipidomics in health and disease: Achievements, challenges and hopes. *Free Radical Biol. Med.* **2017**, *111*, 25−37.
(8) Gaschler, M. M.; Stockwell, B. R. Lipid peroxidation in cell death. *Biochem. Biophys. Res. Commun.* **2017**, *482*, 419−425.
(9) Wong-ekkabut, J.; Xu, Z.; Triampo, W.; Tang, I.-M.; Tieleman, D. P.; Monticelli, L. Effect of lipid peroxidation on the properties of lipid bilayers: a molecular dynamics study. *Biophys. J.* **2007**, *93*, 4225−4236.
(10) Garrec, J.; Monari, A.; Assfeld, X.; Mir, L. M.; Tarek, M. Lipid Peroxidation in Membranes: The Peroxyl Radical Does Not "Float". *J. Phys. Chem. Lett.* **2014**, *5*, 1653−1658.
(11) Weber, G.; Charitat, T.; Baptista, M. S.; Uchoa, A. F.; Pavani, C.; Junqueira, H. C.; Guo, Y.; Baulin, V. A.; Itri, R.; Marques, C. M.; Schroder, A. P. Lipid oxidation induces structural changes in biomimetic membranes. *Soft Matter* **2014**, *10*, 4241−4247.
(12) De Rosa, R.; Spinozzi, F.; Itri, R. Hydroperoxide and carboxyl groups preferential location in oxidized biomembranes experimentally determined by small angle X-ray scattering: Implications in membrane structure. *Biochim. Biophys. Acta, Biomembr.* **2018**, *1860*, 2299−2307.
(13) Siani, P.; de Souza, R. M.; Dias, L. G.; Itri, R.; Khandelia, H. An overview of molecular dynamics simulations of oxidized lipid systems, with a comparison of ELBA and MARTINI force fields for coarse grained lipid simulations. *Biochim. Biophys. Acta* **2016**, *1858*, 2498−2511.
(14) Corvalán, N. A.; Caviglia, A. F.; Felsztyna, I.; Itri, R.; Lascano, R. Lipid Hydroperoxidation Effect on the Dynamical Evolution of the Conductance Process in Bilayer Lipid Membranes: A Condition Toward Criticality. *Langmuir* **2020**, *36*, 8883−8893.
(15) Yusupov, M.; Van der Paal, J.; Neyts, E. C.; Bogaerts, A. Synergistic effect of electric field and lipid oxidation on the permeability of cell membranes. *Biochim. Biophys. Acta, Gen. Subj.* **2017**, *1861*, 839−847.
(16) Rems, L.; Viano, M.; Kasimova, M. A.; Miklavčič, D.; Tarek, M. The contribution of lipid peroxidation to membrane permeability in electropermeabilization: A molecular dynamics study. *Bioelectrochemistry* **2019**, *125*, 46−57.
(17) Itri, R.; Junqueira, H. C.; Mertins, O.; Baptista, M. S. Membrane changes under oxidative stress: the impact of oxidized lipids. *Biophys. Rev.* **2014**, *6*, 47−61.
(18) Melo, A. M.; Ricardo, J. C.; Fedorov, A.; Prieto, M.; Coutinho, A. Fluorescence detection of lipid-induced oligomeric intermediates involved in lysozyme ″amyloid-like″ fiber formation driven by anionic membranes. *J. Phys. Chem. B* **2013**, *117*, 2906−2917.
(19) Melo, A. M.; Loura, L. M. S.; Fernandes, F.; Villalaín, J.; Prieto, M.; Coutinho, A. Electrostatically driven lipid-lysozyme mixed fibers display a multilamellar structure without amyloid features. *Soft Matter* **2014**, *10*, 840−850.
(20) McClare, C. W. An accurate and convenient organic phosphorus assay. *Anal. Biochem.* **1971**, *39*, 527−530.
(21) Pinto, S. N.; Silva, L. C.; de Almeida, R. F. M.; Prieto, M. Membrane domain formation, interdigitation, and morphological alterations induced by the very long chain asymmetric C24:1 ceramide. *Biophys. J.* **2008**, *95*, 2867−2879.
(22) Mazeres, S.; Joly, E.; Lopez, A.; Tardin, C. Characterization of M-laurdan, a versatile probe to explore order in lipid membranes. *F1000Res.* **2014**, *3*, 172.
(23) Glatter, O.; Kratky, O., *Small angle X-ray scattering*; Academic Press: London, 1982.
(24) Frühwirth, T.; Fritz, G.; Freiberger, N.; Glatter, O. Structure and order in lamellar phases determined by small-angle scattering. *J. Appl. Crystallogr.* **2004**, *37*, 703−710.
(25) Kim, H. S.; Martel, A.; Girard, E.; Moulin, M.; Härtlein, M.; Madern, D.; Blackledge, M.; Franzetti, B.; Gabel, F. SAXS/SANS on Supercharged Proteins Reveals Residue-Specific Modifications of the Hydration Shell. *Biophys. J.* **2016**, *110*, 2185−2194.
(26) Gabel, F.; Engilberge, S.; Pérez, J.; Girard, E. Medical contrast media as possible tools for SAXS contrast variation. *IUCrJ* **2019**, *6*, 521−525.
(27) Domingues, M. M.; Bianconi, M. L.; Barbosa, L. R. S.; Santiago, P. S.; Tabak, M.; Castanho, M. A. R. B.; Itri, R.; Santos, N. C. rBPI21 interacts with negative membranes endothermically promoting the formation of rigid multilamellar structures. *Biochim. Biophys. Acta* **2013**, *1828*, 2419−2427.
(28) Zhang, R.; Tristram-Nagle, S.; Sun, W.; Headrick, R. L.; Irving, T. C.; Suter, R. M.; Nagle, J. F. Small-angle x-ray scattering from lipid bilayers is well described by modified Caillé theory but not by paracrystalline theory. *Biophys. J.* **1996**, *70*, 349−357.
(29) Spinozzi, F.; Ferrero, C.; Ortore, M. G.; De Maria Antolinos, A.; Mariani, P. *GENFIT*: software for the analysis of small-angle X-ray and neutron scattering data of macro-molecules in solution. *J. Appl. Crystallogr.* **2014**, *47*, 1132−1139.
(30) Spinozzi, F.; Paccamiccio, L.; Mariani, P.; Amaral, L. Q. Melting regime of the anionic phospholipid DMPG: new lamellar phase and porous bilayer model. *Langmuir* **2010**, *26*, 6484−6493.
(31) Rappolt, M.; Pabst, G.; Amenitsch, H.; Laggner, P. Salt-induced phase separation in the liquid crystalline phase of phosphatidylcholines. *Colloids Surf., A* **2001**, *183-185*, 171−181.
(32) Lakowicz, J. R., *Principles of Fluorescence Spectroscopy*; Springer: New York, 2006.
(33) Melo, A. M.; Fedorov, A.; Prieto, M.; Coutinho, A. Exploring homo-FRET to quantify the oligomer stoichiometry of membrane-bound proteins involved in a cooperative partition equilibrium. *Phys. Chem. Chem. Phys.* **2014**, *16*, 18105−18117.
(34) Kinosita, K., Jr.; Kawato, S.; Ikegami, A. A theory of fluorescence polarization decay in membranes. *Biophys. J.* **1977**, *20*, 289−305.
(35) Kinosita, K., Jr.; Ikegami, A.; Kawato, S. On the wobbling-in-cone analysis of fluorescence anisotropy decay. *Biophys. J.* **1982**, *37*, 461−464.
(36) Prendergast, F. G.; Haugland, R. P.; Callahan, P. J. 1-[4-(Trimethylamino)phenyl]-6-phenylhexa-1,3,5-triene: synthesis, fluorescence properties, and use as a fluorescence probe of lipid bilayers. *Biochemistry* **1981**, *20*, 7333−7338.

https://doi.org/10.1021/acs.langmuir.1c00830
Langmuir 2021, 37, 9952−9963

(37) Mateo, C. R.; Souto, A. A.; Amat-Guerri, F.; Acuña, A. U. New fluorescent octadecapentaenoic acids as probes of lipid membranes and protein-lipid interactions. *Biophys. J.* **1996**, *71*, 2177−2191.
(38) Kinosita, K., Jr.; Kawato, S.; Ikegami, A. Dynamic structure of biological and model membranes: analysis by optical anisotropy decay measurement. *Adv. Biophys.* **1984**, *17*, 147−203.
(39) Mateo, C. R.; Lillo, M. P.; Brochon, J. C.; Martinez-Ripoll, M.; Sanz-Aparicio, J.; Acuna, A. U. Rotational dynamics of 1,6-diphenyl-1,3,5-hexatriene and derivatives from fluorescence depolarization. *J. Phys. Chem.* **1993**, *97*, 3486−3491.
(40) Parasassi, T.; De Stasio, G.; Ravagnan, G.; Rusch, R. M.; Gratton, E. Quantitation of lipid phases in phospholipid vesicles by the generalized polarization of Laurdan fluorescence. *Biophys. J.* **1991**, *60*, 179−189.
(41) Jurkiewicz, P.; Sýkora, J.; Ol żyńska, A.; Humpolíčková, J.; Hof, M. Solvent relaxation in phospholipid bilayers: principles and recent applications. *J. Fluoresc.* **2005**, *15*, 883−894.
(42) Pokorna, S.; Jurkiewicz, P.; Cwiklik, L.; Vazdar, M.; Hof, M. Interactions of monovalent salts with cationic lipid bilayers. *Faraday Discuss.* **2013**, *160*, 341−358 discussion 389-403.
(43) Amaro, M.; Reina, F.; Hof, M.; Eggeling, C.; Sezgin, E. Laurdan and Di-4-ANEPPDHQ probe different properties of the membrane. *J. Phys. D: Appl. Phys.* **2017**, *50*, 134004.
(44) Fee, R. S.; Maroncelli, M. Estimating the time-zero spectrum in time-resolved emmsion measurements of solvation dynamics. *Chem. Phys.* **1994**, *183*, 235−247.
(45) Horng, M. L.; Gardecki, J. A.; Papazyan, A.; Maroncelli, M. Subpicosecond Measurements of Polar Solvation Dynamics: Coumarin 153 Revisited. *J. Phys. Chem.* **1995**, *99*, 17311−17337.
(46) Kučerka, N.; Nieh, M.-P.; Katsaras, J. Fluid phase lipid areas and bilayer thicknesses of commonly used phosphatidylcholines as a function of temperature. *Biochim. Biophys. Acta* **2011**, *1808*, 2761−2771.
(47) Pabst, G.; Hodzic, A.; Štrancar, J.; Danner, S.; Rappolt, M.; Laggner, P. Rigidification of neutral lipid bilayers in the presence of salts. *Biophys. J.* **2007**, *93*, 2688−2696.
(48) Chu, N.; Kučerka, N.; Liu, Y.; Tristram-Nagle, S.; Nagle, J. F. Anomalous swelling of lipid bilayer stacks is caused by softening of the bending modulus. *Phys. Rev. E* **2005**, *71*, No. 041904.
(49) Bouvrais, H.; Duelund, L.; Ipsen, J. H. Buffers affect the bending rigidity of model lipid membranes. *Langmuir* **2014**, *30*, 13−16.
(50) Ayee, M. A. A.; LeMaster, E.; Shentu, T. P.; Singh, D. K.; Barbera, N.; Soni, D.; Tiruppathi, C.; Subbaiah, P. V.; Berdyshev, E.; Bronova, I.; Cho, M.; Akpa, B. S.; Levitan, I. Molecular-Scale Biophysical Modulation of an Endothelial Membrane by Oxidized Phospholipids. *Biophys. J.* **2017**, *112*, 325−338.
(51) Kang, T.; Qian, S.; Smith, G. S.; Do, C.; Heller, W. T. Small-angle neutron scattering study of a dense microemulsion system formed with an ionic liquid. *Soft Matter* **2017**, *13*, 7154−7160.
(52) Rekvig, L.; Hafskjold, B.; Smit, B. Chain length dependencies of the bending modulus of surfactant monolayers. *Phys. Rev. Lett.* **2004**, *92*, 116101.
(53) do Canto, A. M. T. M.; Robalo, J. R.; Santos, P. D.; Carvalho, A. J. P.; Ramalho, J. P. P.; Loura, L. M. S. Diphenylhexatriene membrane probes DPH and TMA-DPH: A comparative molecular dynamics simulation study. *Biochim. Biophys. Acta* **2016**, *1858*, 2647−2661.
(54) van Langen, H.; van Ginkel, G.; Shaw, D.; Levine, Y. K. The fidelity of response by 1-[4-(trimethylammonio)phenyl]-6-phenyl-1,3,5-hexatriene in time-resolved fluorescence anisotropy measurements on lipid vesicles. Effects of unsaturation, headgroup and cholesterol on orientational order and reorientational dynamics. *Eur. Biophys. J.* **1989**, *17*, 37−48.
(55) Muller, J. M.; van Faassen, E. E.; van Ginkel, G. Experimental support for a novel compound motion model for the time-resolved fluorescence anisotropy decay of TMA-PDH in lipid vesicle bilayers. *Chem. Phys.* **1994**, *185*, 393−404.
(56) Straume, M.; Litman, B. J. Equilibrium and dynamic bilayer structural properties of unsaturated acyl chain phosphatidylcholine-cholesterol-rhodopsin recombinant vesicles and rod outer segment disk membranes as determined from higher order analysis of fluorescence anisotropy decay. *Biochemistry* **1988**, *27*, 7723−7733.
(57) Gracetto, A. C.; Batistela, V. R.; Caetano, W.; de Oliveira, H. P. M.; Santos, W. G.; Cavalheiro, C. C. S.; Hioka, N. Unusual 1,6-diphenyl-1,3,5-hexatriene (DPH) spectrophotometric behavior in water/ethanol and water/DMSO mixtures. *J. Braz. Chem. Soc.* **2010**, *21*, 1497−1502.
(58) Parasassi, T.; De Stasio, G.; Rusch, R. M.; Gratton, E. A photophysical model for diphenylhexatriene fluorescence decay in solvents and in phospholipid vesicles. *Biophys. J.* **1991**, *59*, 466−475.
(59) Sutter, M.; Fiechter, T.; Imanidis, G. Correlation of membrane order and dynamics derived from time-resolved fluorescence measurements with solute permeability. *J. Pharm. Sci.* **2004**, *93*, 2090−2107.
(60) Vyšniauskas, A.; Qurashi, M.; Kuimova, M. K. A Molecular Rotor that Measures Dynamic Changes of Lipid Bilayer Viscosity Caused by Oxidative Stress. *Chemistry* **2016**, *22*, 13210−13217.
(61) Volinsky, R.; Cwiklik, L.; Jurkiewicz, P.; Hof, M.; Jungwirth, P.; Kinnunen, P. K. J. Oxidized phosphatidylcholines facilitate phospholipid flip-flop in liposomes. *Biophys. J.* **2011**, *101*, 1376−1384.
(62) Först, G.; Cwiklik, L.; Jurkiewicz, P.; Schubert, R.; Hof, M. Interactions of beta-blockers with model lipid membranes: molecular view of the interaction of acebutolol, oxprenolol, and propranolol with phosphatidylcholine vesicles by time-dependent fluorescence shift and molecular dynamics simulations. *Eur. J. Pharm. Biopharm.* **2014**, *87*, 559−569.
(63) Kulig, W.; Olżyńska, A.; Jurkiewicz, P.; Kantola, A. M.; Komulainen, S.; Manna, M.; Pourmousa, M.; Vazdar, M.; Cwiklik, L.; Rog, T.; Khelashvili, G.; Harries, D.; Telkki, V. V.; Hof, M.; Vattulainen, I.; Jungwirth, P. Cholesterol under oxidative stress-How lipid membranes sense oxidation as cholesterol is being replaced by oxysterols. *Free Radical Biol. Med.* **2015**, *84*, 30−41.
(64) Jurkiewicz, P.; Olżyńska, A.; Langner, M.; Hof, M. Headgroup Hydration and Mobility of DOTAP/DOPC Bilayers: A Fluorescence Solvent Relaxation Study. *Langmuir* **2006**, *22*, 8741−8749.
(65) Conte, E.; Bardi, E.; Losito, I.; Annese, C.; Ciminale, F.; Megli, F. M. Does hydrogen bonding contribute to lipoperoxidation-dependent membrane fluidity variation? An EPR-spin labeling study. *Biochim. Biophys. Acta* **2015**, *1848*, 2040−2049.

https://doi.org/10.1021/acs.langmuir.1c00830
Langmuir 2021, 37, 9952−9963